Anderson William Jr, RE Emanuel (2010) Effect of interannual climate oscillations on rates of submarine groundwater discharge, Water Resource Res 46:W05503, doi:10.1029/2009WR008212.
Version of record available from Wiley [ISSN: 1944-7973], [DOI: 10.1029/2009WR008212]

Effect of interannual climate oscillations on rates of submarine groundwater discharge

Abstract

[1] Submarine groundwater discharge (SGD) is an important component of the coastal hydrologic cycle, affecting mixing and biogeochemistry in the nearshore environment. El Niño–Southern Oscillation (ENSO) influences rates of precipitation and groundwater recharge in many regions, including barrier islands of the southeastern U.S. coast; however, the influence of ENSO on SGD is poorly understood for this region. Here we investigate the role of ENSO in controlling recharge and SGD at interannual time scales, using modeling results for both real and generic barrier island environments. Results of our 57 year simulations show that the freshwater component of seasonally averaged SGD as well as groundwater discharge velocity, water table elevation, and submarine groundwater recharge are significantly correlated with ENSO for a real barrier island (Hatteras Island, North Carolina) and, under certain conditions, for generics. These correlations persist for lag times as great as 5 months during winter, creating anomalies of up to 35% between El Niño and La Niña conditions and suggesting that both hydrologic cycling and biogeochemical cycling in these systems are significantly influenced by ENSO.

1. Introduction

[2] Interactions between groundwater and surface water have been well studied over the past few decades. For example, studies of heat flow by *Suzuki* [1960] and *Stallman* [1965] have led to the use of temperature data to quantify groundwater-stream interactions. Although studies of coastal groundwater–surface water interactions extend back to the same time period [e.g., *Kohout*, 1960], *Taniguchi et al.* [2002] suggest that only recently have coastal interactions such as submarine groundwater discharge (SGD) received adequate attention. SGD is an important component of the global water balance [*Li et al.*, 1999], and estimates of the rate of SGD have broad implications for the transfer of surface-based pollutants through the nearshore environment [*Li et al.*, 1999] and biogeochemical cycling within coastal systems [*Smith et al.*, 2008]. Seminal research on this subject has been conducted by *Moore* [1996, 1999], who describes a subterranean estuary in which fresh groundwater and saline ocean circulation intersect. Since that research, much work has gone into characterizing and quantifying rates of SGD and submarine groundwater recharge (SGR) at multiple spatial and temporal scales. For example, *Wilson* [2003] describes the large-scale circulation of seawater within the continental shelf, while *Moore et al.* [2002] describe localized variations in SGD based on temperature measurements in submarine wells. Both *Taniguchi et al.* [2002] and *Burnett et al.* [2006] summarize the methods used to quantify SGD. Several of these methods have been applied in the field (see, e.g., *Michael et al.* [2003] and *Mulligan and Charette* [2006] for the use of various methods in Waquoit Bay, Massachusetts).

[3] Waves, tides, storms, and seasonal variations have all been shown to affect the rates of SGD. *Li et al.* [1999] suggested that up to 96% of total SGD is marine water recirculating through the nearshore by the processes of wave setup and tidal oscillations, leaving a balance of land-based freshwater contribution of 4%. *Moore et al.* [2002] demonstrated the influence of tidal oscillations in temperature variations that are in phase with the tidal signal in submarine wells 20 km off of the coast of North Carolina. These oscillations indicate that tides can play a large role in the circulation of fluids in the near surface of coastal aquifers, even at significant distances from the shoreline. *Taniguchi* [2002] collected detailed measurements of SGD rates in Osaka Bay, Japan, over the course of approximately 5 months. He detected decreasing rates of SGD as tidal levels increase, and vice versa, suggesting that tidal oscillations have a direct influence on SGD. *Prieto and Destouni* [2005] used modeling studies of several islands in the Mediterranean Sea to determine that tidal oscillations have the most effect in areas of low SGD, where they help to drive SGD circulation; however, they also showed that high rates of SGD must be accompanied by large freshwater circulation from adjacent land. Tidal pumping and storm events drive the temperature fluctuations in offshore wells that *Moore and Wilson* [2005] have attributed to the exchange of pore water. Other studies have examined the influence of episodic storm events on groundwater flow in the nearshore environment. *Smith et al.* [2008], documenting the effect of two tropical storm events

Table 1. Seasonal Recharge Fractions

Season	Mean	Standard Deviation
Winter	0.562	0.165
Spring	0.621	0.262
Summer	0.356	0.094
Autumn	0.375	0.124

on rates of SGD, suggested that these storms affect the location and biogeochemistry of the subterranean estuary. *Anderson and Lauer* [2008] detailed the influence of hurricanes and tropical storms on the morphology of the subterranean estuary, finding that episodic storm events might affect this mixing zone on the order of years. *Michael et al.* [2005] documented seasonal oscillations in rates of SGD. Using field observations and modeling, they demonstrated variations in the location of the freshwater-saltwater interface that lag seasonal recharge patterns.

[4] This research summary demonstrates that periodic forcing factors control SGD at several time scales; however, the impact of deviations from simple periodicity has not been studied to date, especially at interannual time scales. For example, in many regions, especially those dominated by interannual climate oscillations, a seasonal model of recharge variation that drives freshwater SGD may not be appropriate. Potential evapotranspiration may exhibit a seasonal periodicity [*Anderson and Evans*, 2007], but in regions affected by interannual and interdecadal climate signals, precipitation, and therefore recharge, will vary according to available moisture [*Anderson and Emanuel*, 2008]. Thus, although potential evapotranspiration will typically be low during the winter season, climate conditions may limit the amount of precipitation, thereby producing low recharge rates when high recharge rates are expected. Conversely, although potential evapotranspiration will typically be high in the summer season, large amounts of precipitation could still result in high recharge, especially in response to extreme storm events [*Anderson and Lauer*, 2008].

[5] Although a periodic recharge model may apply to some aquifers, this will not be the case in all regions, especially those affected by interannual climate oscillations. Multiyear climate oscillations such as the El Niño–Southern Oscillation (ENSO) and Pacific Decadal Oscillation (PDO) affect precipitation and stream discharge rates in the Western Hemisphere [*Beebee and Manga*, 2004; *D'Odorico et al.*, 2001; *Rajagopalan and Lall*, 1998]. Recent studies have extended these relationships to the groundwater reservoir. *Rodell and Famiglietti* [2001] have hypothesized that there is a connection between climate oscillations and groundwater resource availability. Several studies in western North America and the Pacific relate groundwater conditions to various climate signals [*Drexler and Ewel*, 2001; *Hanson et al.*, 2004; *Fleming and Quilty*, 2006; *van der Velde et al.*, 2006]. In the southeastern United States in the general region of the current study, *Anderson and Emanuel* [2008] analyzed 56 years of precipitation data from 94 stations to demonstrate significant correlation between winter ENSO conditions and winter precipitation. They observed an anomaly of up to 67% more winter precipitation during strong El Niño conditions than during strong La Niña conditions and found that the magnitude of the anomaly decreases with distance from the Atlantic coast. The precipitation anomaly demonstrated by *Anderson and Emanuel* [2008] extends to the groundwater reservoir, where winter base flow is also influenced by ENSO at a lag of up to 3 months.

[6] Herein, we use modeling studies to demonstrate that the ENSO signal that affects base flow in this region also influences the morphology of the mixing zone in coastal aquifers along this coast, and that this signal may also affect SGD and SGR in coastal aquifers within this and other ENSO-correlative regions (see *Kurtzman and Scanlon* [2007] for details on these regions). It is our aim with this paper to document the potential influence of interannual climate oscillations on SGD and to estimate the seasonal correlations, magnitudes of impact (anomalies), and lag times of this phenomenon in coastal aquifer systems. We follow the methodology of *Anderson and Emanuel* [2008] and compare time series of model output with that of the Multivariate ENSO Index (MEI) [*Wolter and Timlin*, 1998]. MEI derives from the Comprehensive Ocean-Atmosphere Data Set and uses six observations measured over the tropical Pacific Ocean (sea level pressure, surface zonal wind, meridional wind, sea surface temperature, surface air temperature, and cloudiness). The MEI represents normalized bimonthly means relative to a base period. Positive values correspond to El Niño conditions; negative values correspond to La Niña conditions [*Wolter and Timlin*, 1998].

2. Modeling Methods

[7] We use numerical modeling techniques to examine the effect of ENSO-induced precipitation variations on groundwater–surface water interactions in the nearshore environment. This research utilizes modeling methods because of the lack of long-term (i.e., multidecadal) time series of SGD and SGR rates, which in the literature extend only to the tidal [e.g., *Taniguchi*, 2002] and seasonal [e.g., *Michael et al.*, 2005] temporal scales. Observed precipitation drives the magnitude of the seasonal recharge rates in our simulations; therefore, the correlations between the modeling results and MEI are emergent and are not specified a priori.

[8] Observed precipitation influences the model through the modeled seasonal recharge rates. Detailed time series of water table elevations were observed in monitoring wells on Hatteras Island over a period of 6 years (1993–1995 and 2001–2004). (See *Anderson and Evans* [2007, their Figure 5] for a water table hydrograph of the 2001–2004 data; seasonal means of these water table hydrographs are shown here in Figure 4 (bottom) and in Figure 5.) We calibrated steady state SUTRA simulations to these observed seasonal-mean water table elevations, thereby generating mean seasonal recharge rates (e.g., December–January–February for winter, March–April–May for spring, etc.). For each seasonal simulation we determined the seasonal recharge fraction, which is the ratio of the total simulated recharge during that season to the total observed precipitation during that season. Table 1 lists the statistics generated from these recharge fraction calibrations.

[9] These precipitation-derived recharge fractions were used to generate a 57 year recharge signal (228 distinct seasons) through a random sampling of the calibrated seasonal recharge fractions based on the data in Table 1. The 228 random seasonal recharge fractions were then multiplied by the observed seasonal precipitation totals to produce the recharge rate for each season. The random

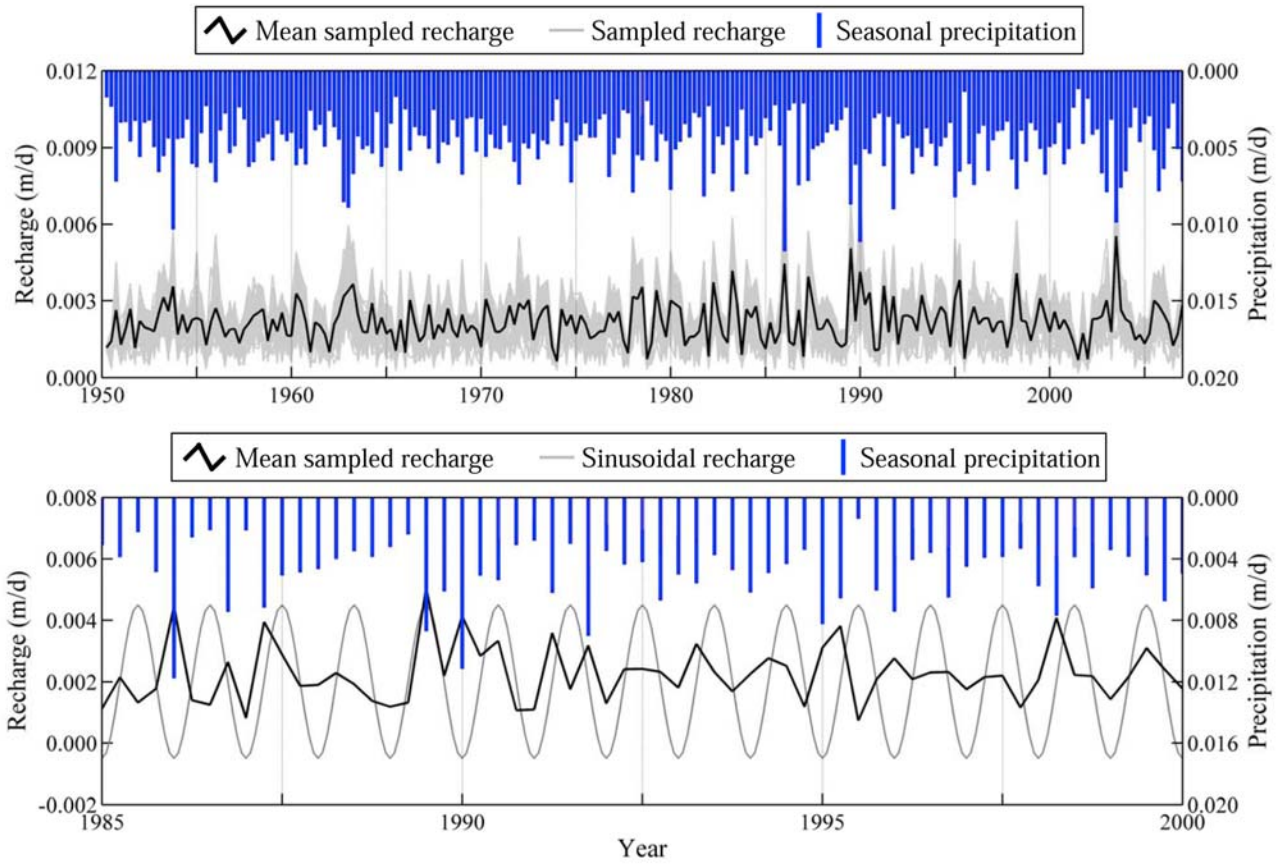

Figure 1. (top) The results of Monte Carlo sampling of 500 realizations of seasonal recharge fractions by the seasonal precipitation total. Realizations are shown in gray, the mean of the realizations is shown in black, and both are plotted using the left vertical axis. Vertical bars indicate seasonal precipitation totals using the reversed right vertical axis. (bottom) A comparison of the mean seasonal recharge as calculated from the 500 Monte Carlo realizations (black line) and the periodic recharge signal of *Michael et al.* [2005] (gray line). Both are plotted using the left vertical axis. Vertical bars indicate seasonal precipitation totals using the reversed right vertical axis.

sampling of the recharge fraction was employed because of the relatively large standard deviations in the recharge fractions. We utilized a Monte Carlo sampling process (100 realizations) to account for this observed variation in seasonal recharge fractions. The model output consists of seasonal time series because we are interested in the seasonal correlation between the model-generated SGD rates and seasonal means of the MEI, a methodology similar to that employed by *Kurtzman and Scanlon* [2007] and *Anderson and Emanuel* [2008].

[10] Figure 1 (top), which compares randomly generated seasonal recharge rates from the previously described Monte Carlo simulation (500 realizations in gray with the mean of these realizations in black) with the observed seasonal precipitation (vertical bars), demonstrates that peaks in recharge correspond to peaks in observed precipitation. Figure 1 (bottom) compares the mean of the seasonal recharge signal and the observed seasonal precipitation to a periodic signal based on the work of *Michael et al.* [2005]. We zoom to the years 1985 through 2000 to demonstrate the differences between these time series. While the random seasonal and periodic recharge signals are sometimes in phase, in many instances the signals are either significantly out of phase or lack significant oscillation. There is also no observable correlation between the observed seasonal precipitation and the periodic recharge signal. We further explore the periodicity of the randomly generated seasonal recharge and the observed seasonal precipitation in section 3.

[11] December 1949 corresponds with the initial date of the bimonthly average MEI (accessed from http://www.cdc.noaa.gov/people/klaus.wolter/MEI/table.html during November 2007). To maintain consistency with the MEI signal, we convert simulated seasonal water table elevation, discharge velocity, SGD, and SGR to bimonthly averages, then convert these simulation results and the MEI signal to seasonal averages. We compare seasonal model output to seasonal MEI using Spearman's rank correlation (ρ) and calculate seasonal anomalies in the model output between the upper quartile of positive and the lower quartile of negative extremes in the MEI following *Kurtzman and Scanlon* [2007].

2.1. Hatteras Island Model

[12] Hatteras Island is a barrier island in the Outer Banks of North Carolina, lying approximately 35 km from mainland North Carolina (Figure 2, top). It is bordered to the north and west by Pamlico Sound, which is a 3100 km^2 estuary, and on the south and east by the Atlantic Ocean.

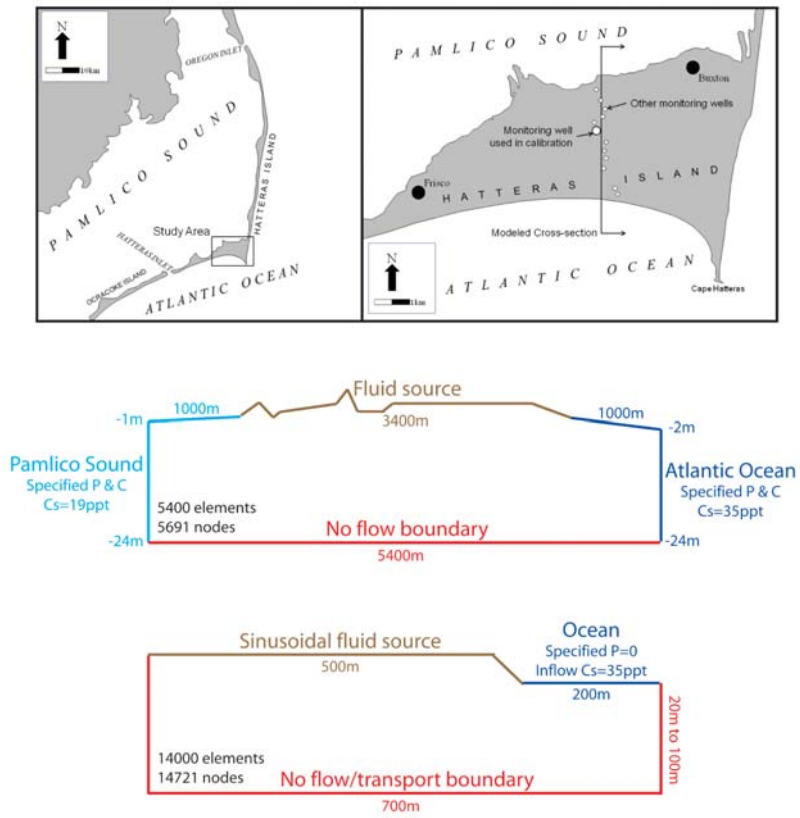

Figure 2. (top) Location of the Hatteras Island study site. (middle) Model domain for simulations performed along a cross section of Hatteras Island, North Carolina. (bottom) Model domain for simulations performed with the generic model, based on the model domain of *Michael et al.* [2005]. Specified P & C refers to specified pressure and concentration boundary conditions. Cs refers to the concentration of the source.

The study site lies at the point where the island shifts from a north-south trend to an east-west trend. At this point the island is approximately 3400 m in width. The surficial aquifer of Hatteras Island comprises 24 m of medium- to coarse-grained sand with shell fragments and a 3 m section between depths of 12 to 15 m made up of fine-grained sands and silts. The aquifer is underlain by a 13 m sequence of silty to clayey sand [*Anderson et al.*, 2000], which we designate as a no-flow boundary.

[13] *Anderson and Lauer* [2008] described the long-term influence of extreme storm events on the surficial aquifer of Hatteras Island with a series of groundwater flow and solute transport simulations, utilizing the U.S. Geological Survey finite element model SUTRA [*Voss*, 1984; *Voss and Provost*, 2002], a model used in other SGD studies [e.g., *Li et al.*, 2000; *Smith*, 2004; *Wilson and Gardner*, 2006]. We use the model domain of *Anderson and Lauer* [2008] to investigate the influence of ENSO-driven recharge variations since 1950 on the rate of SGD and SGR in the nearshore environments of the Atlantic Ocean and Pamlico Sound offshore of Hatteras Island (Figure 2, middle). *Anderson and Lauer* [2008], using known hydrogeology [*Anderson et al.*, 2000] and aquifer parameters [*Burkett*, 1996], calibrated dispersion parameters to breakthrough curves of total dissolved solids derived from hurricane overwash. We use these calibrated parameters, the stochastically generated recharge rates described above, and the two-dimensional model domain, consisting of 5671 nodes and 5381 elements, to simulate long-term variations in the location of the mixing zone (Table 2). The simulations use an island width of 3400 m and extend the simulated nearshore 1000 m into Pamlico Sound (mass concentration of 0.019 kg/kg) and the Atlantic Ocean (mass concentration of 0.0357 kg/kg). Both lateral boundaries of the model domain are set at fixed pressures. In our simulations, we ignore tidal oscillations and wave runup, as do *Michael et al.* [2005]. While simulated rates of freshwater SGD are low relative to those suggested for wave runup and tidal oscillations [*Li et al.*, 1999], we point

Table 2. Hatteras Island and Generic Model Parameters

Parameter	Value
Hatteras Island Model	
Maximum permeability (m^2)	2.7×10^{-11}
Minimum permeability (m^2)	6.6×10^{-12}
Generic Model	
Maximum and minimum permeability (m^2)	1.0×10^{-11}
Both Models	
Porosity	0.20
Recharge (kg/s)	variable
Longitudinal dispersivity in maximum permeability direction (m)	10
Longitudinal dispersivity in minimum permeability direction (m)	5
Transverse dispersivity in maximum permeability direction (m)	1
Transverse dispersivity in minimum permeability direction (m)	1
Model thickness (m)	1.0

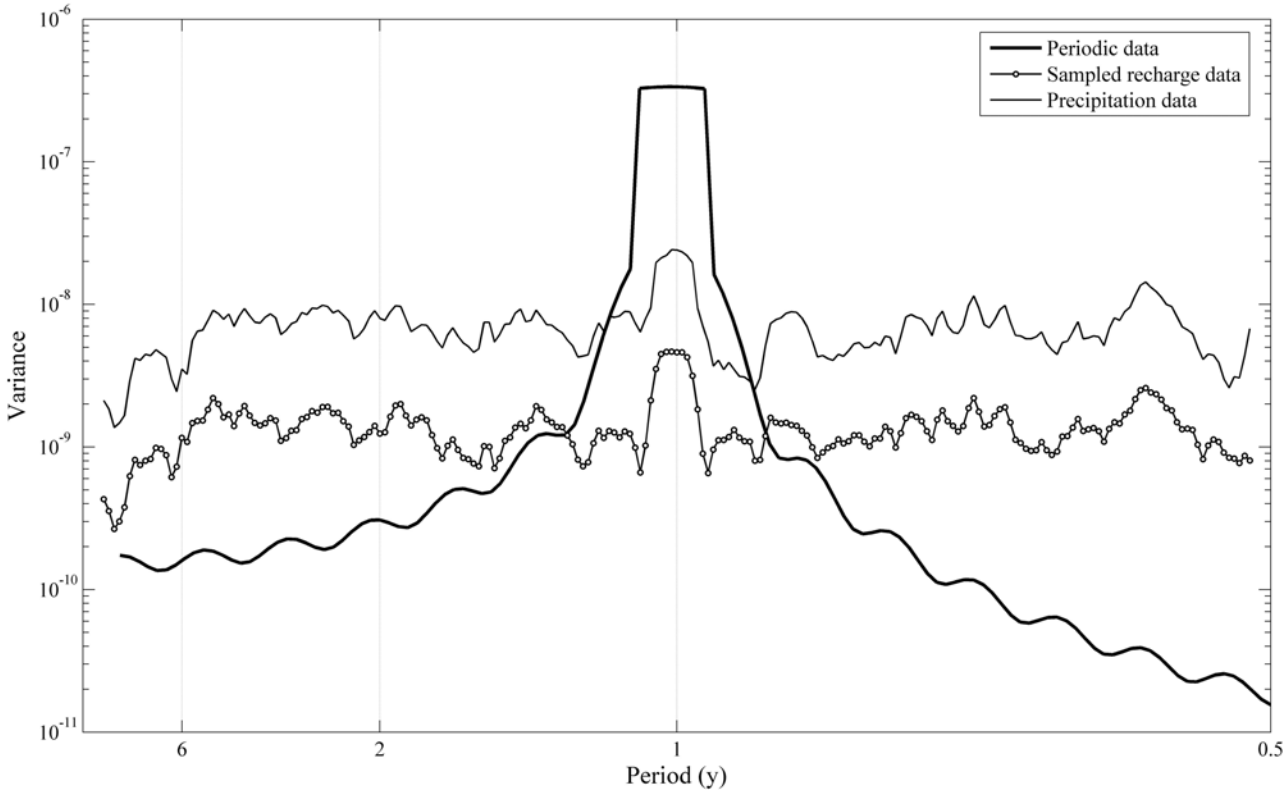

Figure 3. A periodogram of a periodic recharge signal (thick black line), the mean of the randomly sampled recharge signal for Hatteras Island (thin black line with white circles), and measured seasonal precipitation for Hatteras Island (thin black line). The horizontal axis is shown in terms of period (*y*). The vertical axis is shown in terms of variance (m^2/d^2). The original calculations produced the unsmoothed variance spectrum of each time series, which was then smoothed using a running average. Windowing was not used in the construction of the periodogram.

out that freshwater SGD constitutes the primary mechanism by which contaminants enter the coastal ocean.

[14] We randomly generate seasonal recharge rates for the years 1950 through 2006, using the methodology described above to test the influence of variable recharge rates on the freshwater-saltwater interface. To address uncertainty in these calculations, we use a Monte Carlo technique to randomly generate seasonal recharge fractions based on the mean and standard deviation of the calibration simulations. We run 100 realizations with these random seasonal recharge signals and the calibrated parameters of *Anderson and Lauer* [2008] to generate time series of groundwater discharge velocity, SGD, SGR, and water table elevations. These modeled time series are then used to investigate their lagged seasonal correlation with the seasonal ENSO signal as expressed by the MEI [*Wolter and Timlin*, 1998]. To do this, we first compute seasonal averages for both MEI and the hydrologic variables (e.g., winter = average Dec–Jan–Feb value, etc.), and then compare seasonally averaged MEI with each seasonally averaged hydrologic variable, using Spearman's rank correlation. (See *Anderson and Emanuel* [2008] for additional details.) We assess lag correlations between MEI and hydrologic responses by advancing the averaging period for hydrologic variables by 1 month at a time (e.g., comparing winter MEI with average Jan–Feb–Mar values for each hydrologic variable) to obtain Spearman's rank correlation coefficients for lag times of 0 to 5 months.

2.2. Generic Model

[15] To explore the influence of various aquifer parameters on these same correlations, and to further explore the freshwater component of SGD, we also apply this method to the model domain of *Michael et al.* [2005], which was used to demonstrate the seasonal oscillations of SGD (Figure 2, bottom). This study's adaptation of that two-dimensional model domain consists of 14,701 nodes and 13,981 elements and incorporates a land-based 500 m freshwater aquifer that extends 200 m into the simulated nearshore ocean (mass concentration of 0.0357 kg/kg as opposed to the 0.03 kg/kg mass concentration used by *Michael et al.* [2005]). The bottom and lateral boundaries of the model domain are designated as no-flow boundaries. The model uses the same aquifer parameters as those of *Michael et al.* [2005] (Table 2), although coarser grid spacing and quadrilateral elements are employed. The base scenario scales the randomly generated recharge signal we use for the Hatteras Island simulations to the mean recharge used by *Michael et al.* [2005] (Figure 1, bottom). In the subsequent sensitivity study, we vary permeability, recharge, and aquifer thickness to assess the influence of these parameters on ENSO correlations.

3. Results

[16] We begin with spectral analyses of the periodic and randomly generated seasonal recharge and observed sea-

Table 3. Significant ENSO Correlations for $p < 0.05$ for the Hatteras Island Simulations

	Lag (months)					
	0	1	2	3	4	5
Precipitation						
Winter	0.40[a]	0.49	0.28	-	-	−0.28
Spring	-	-	-	-	-	-
WT elevation						
Winter	0.40	0.39	0.34	0.30	-	-
Spring	0.29	-	-	-	-	-
Discharge velocity						
Winter	−0.47	−0.47	−0.42	−0.38	−0.31	−0.29
Spring	−0.40	−0.28	-	-	-	-
SGR						
Winter	0.33	0.32	0.29	0.30	0.30	0.27
Spring	-	-	-	-	-	-

[a]All significant correlations are shown as values of Spearman's ρ.

sonal precipitation signals (Figure 3). As expected, the periodic signal shows the highest variance at a period of 1 year, which is the period of oscillation in the recharge signal, recharge rates being high in late winter/early spring and low in late summer/early fall. The variance at the 1 year period is 3 orders of magnitude greater than it is at other periods. The random seasonal recharge and observed seasonal precipitation signals are significantly different from the periodic recharge signal. Although the largest variance in these signals occurs at a period of 1 year, the magnitude of this variance is only a factor of approximately 2 greater than the variance at adjacent periods. Of additional interest is the slightly higher variance between 2 and 6 year periods, which is the period of oscillation of ENSO [*Hanson et al.*, 2004].

[17] The presentation of the simulation results is based on the work of *Kurtzman and Scanlon* [2007], which was subsequently adapted by *Anderson and Emanuel* [2008]. The upper quartile of the MEI represents the years in which the highest MEI signals occurred (75th percentile) and also those in which the strongest El Niños occurred. Conversely, the lower quartile of the MEI represents the years in which the lowest MEI signals occurred (25th percentile); these years are those in which the strongest La Niñas occurred. When computing anomalies, we calculate the ratio of the mean values of a specific parameter (e.g., water table elevation, freshwater SGD, …), comparing the values in the upper quartile years with those the lower quartile years. For example, *Anderson and Emanuel* [2008] reported a winter base flow anomaly of 100% in the southeastern portion of their study area at 2 months lag, meaning that twice as much base flow occurred during strong positive MEI conditions than during strong negative MEI conditions.

[18] *Anderson and Emanuel* [2008] demonstrate that the Hatteras Island precipitation data correlate strongly with ENSO. Here we extend this work to show lag correlations between 0 and 5 months (Table 3). At this site, winter precipitation is positively correlated with MEI at lag times of between 0 and 2 months. These times of strong correlation also correspond to the time of year when aquifer recharge is typically greatest. Because of this, we argue that winter precipitation is the primary pathway by which the ENSO signal is transmitted into the Hatteras Island aquifer. During these months, the strong correlation between MEI and precipitation together with the relatively high recharge fraction combine to produce an amplified signal of ENSO-induced hydrologic anomalies that propagate through the aquifer.

3.1. Hatteras Island Model

[19] The Hatteras Island simulations are meant to test conditions in a real coastal aquifer system. Aquifer parameters derived from extensive aquifer testing on Hatteras Island have been used in a previous model of the island that calibrated well to water table elevations and salinity levels [*Anderson and Lauer*, 2008]. The significant correlations of precipitation with MEI at multiple lags extend to the simulation results of Hatteras Island and show that ENSO exerts a significant influence on lagged water table elevations, nearshore discharge velocities, and SGR during the winter and spring seasons—a correlation similar not only to those for observed precipitation but also to those found for base flow in eastern and coastal North Carolina by *Anderson and Emanuel* [2008] (Table 3). Correlations during the summer and autumn seasons are not significant and, therefore, are not shown.

[20] Figure 4 shows the results of the Hatteras Island simulations. Model output in the nearshore of Pamlico Sound, being similar to that in the nearshore of the Atlantic Ocean, is not shown. Time series of groundwater discharge velocities in the nearshore of the Atlantic Ocean were generated from the Hatteras Island simulations for each of the 100 Monte Carlo realizations. An overall mean of these time series was also generated and is the time series used in determining the statistical correlations (Figure 4, top). Time series of SGD and SGR in the nearshore of the Atlantic Ocean were also generated for each of the Monte Carlo realizations (Figure 4, middle). Simulated SGD and SGR are inversely proportional, values of SGR being low during periods of high SGD and high during low values of SGD. Total SGD, which is the mean of all of the Monte Carlo realizations, is approximately 3.5 m^2/d, a rate 40% larger than the total SGR mean of 2.5 m^2/d. This is the same order of magnitude as the simulated rates of *Li et al.* [1999] and *Michael et al.* [2005].

[21] Water table elevations were measured during two separate studies in the mid-1990s and the early 2000s. *Anderson and Evans* [2007] show a water table hydrograph of the latter of these field data. A time series of simulated water table elevations was also generated from the Hatteras Island model and compared with the field observations (Figure 4, bottom). Mean seasonal water table elevations are shown in Figure 4 (bottom) to indicate the consistency between the model and the field observations. The mean value of all of the simulated water table elevations is 1.51 m, quite close to the mean of 1.44 m for all of the observed water table measurements. This difference constitutes error of less than 5%, and this error is likely due to the timing of the field measurements, which mostly occurred during wet years. For example, 17 of the seasonal mean observations are above the field mean, whereas only 8 of the seasonal mean observations are below the field mean.

[22] We further evaluate the ability of the model to reproduce field conditions in Figure 5. Figure 5 (top) shows data observed between 1993 and 1996. Daily mean water table elevations compare favorably with the seasonal means that are shown Figure 4 (bottom). The general trend of these high-frequency data is also mimicked well by the modeled seasonal water table elevations, which are able to match all

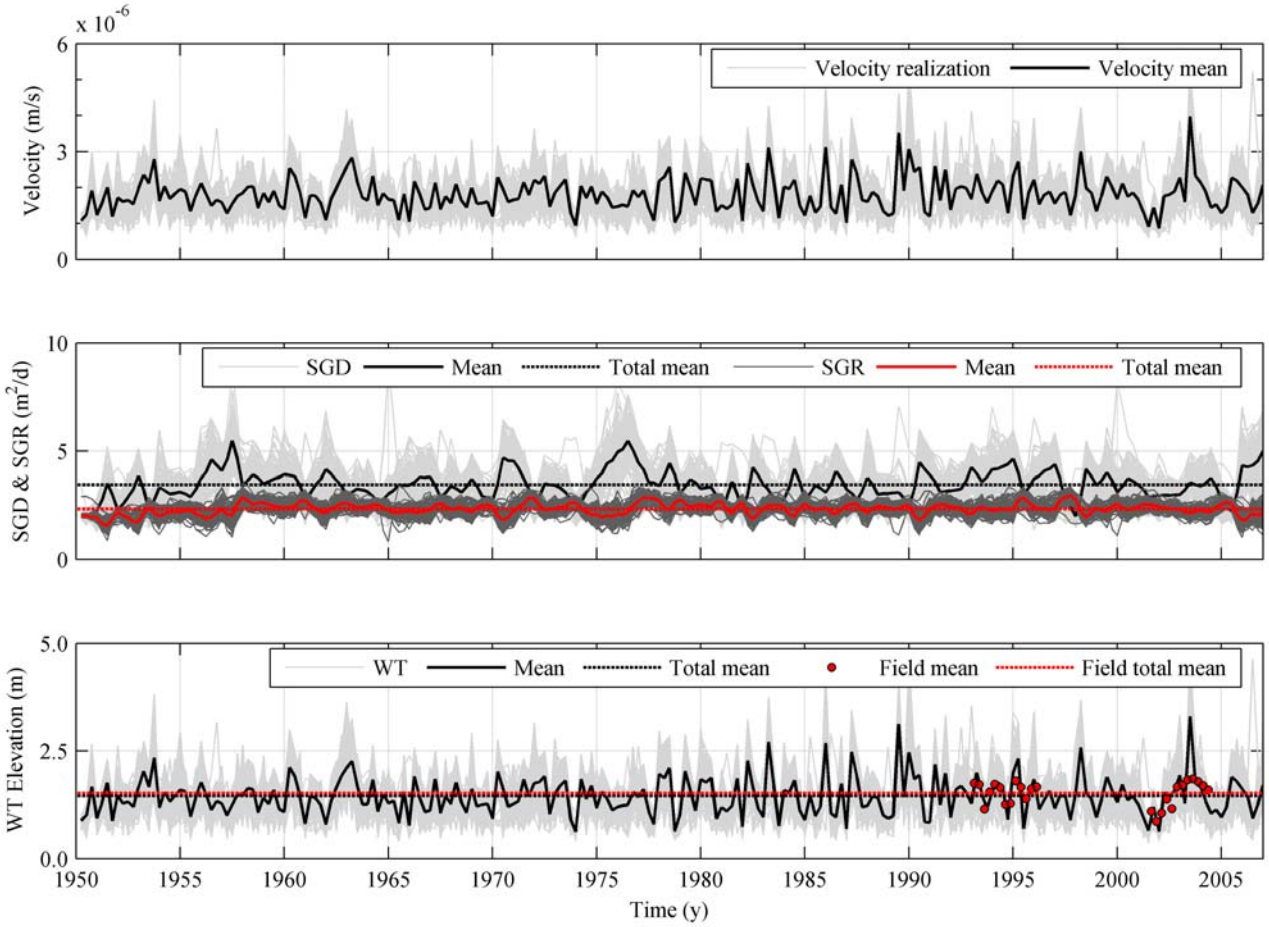

Figure 4. Hatteras Island simulation results. (top) Monte Carlo realizations (gray lines) and mean (black solid line) of simulated groundwater discharge (SGD) velocity at the shoreline of the Atlantic Ocean. (middle) Monte Carlo realizations (SGD, light gray lines; submarine groundwater recharge (SGR), dark gray lines), mean (SGD, solid black line; SGR, solid red line), and total mean (SGD, black dashed line; SGR, red dashed line) of simulated SGD and SGR at the shoreline of the Atlantic Ocean. (bottom) Monte Carlo realizations (gray lines), mean (black solid line), and total mean (black dashed line) of simulated water table (WT) elevations and seasonal (red dots) and total mean (red dashed line) of field-measured data.

portions of the data set except for the suggestion of an overly low water table in mid-1995. Figure 5 (bottom) shows data observed between July 2001 and March 2004. These data represent twice-daily measurements of water table elevations. The timing of these measurements was more interesting than those shown in Figure 5 (top), which are relatively sinusoidal and seem to correspond with the seasonal pattern observed by *Michael et al.* [2005]. Conditions were far from sinusoidal between 2001 and 2004. Water table elevations at the beginning of this measurement period were the lowest ever observed at this site. An abrupt change in the climate signal in mid-2002 from weak La Niña to relatively strong El Niño conditions, however, produced some of the highest water table elevations ever measured at this site, elevations that were sustained through multiple seasons. The modeled seasonal water table elevations match these data well except at two locations. First, several large storm events occurred in mid-2002. Because the model spreads the total seasonal precipitation over the entire season in calculating recharge rates, the model predicts water table elevations at the upper range of observed data. Second, the extended wet conditions during mid-2003 caused the modeled water table elevations to be quite a bit higher than the field data. So much moisture was available during summer 2003 that even with the low summer recharge fraction, the modeled water table elevations were higher than observed.

[23] We report the model correlations (Table 3) in terms of nearshore groundwater discharge velocities because the total SGD signal includes saline circulation, which does not respond to the ENSO signal. Winter correlations are strong at multiple lags. Water table elevations show significant correlations ($p < 0.05$) of up to 3 months lag (Spearman's ρ ranging from 0.40 to 0.30). Water table anomalies indicate variations of 18.9% to 25.6% between 0 and 3 months lag. Simulated groundwater discharge velocities in the nearshore of Pamlico Sound and the Atlantic Ocean show significant correlations of up to 5 months lag (Spearman's ρ ranging from 0.47 to 0.29). Anomalies in groundwater discharge velocity to the Atlantic Ocean indicate variations of 17.6% to 23.8% between 0 and 3 months lag. Anomalies in

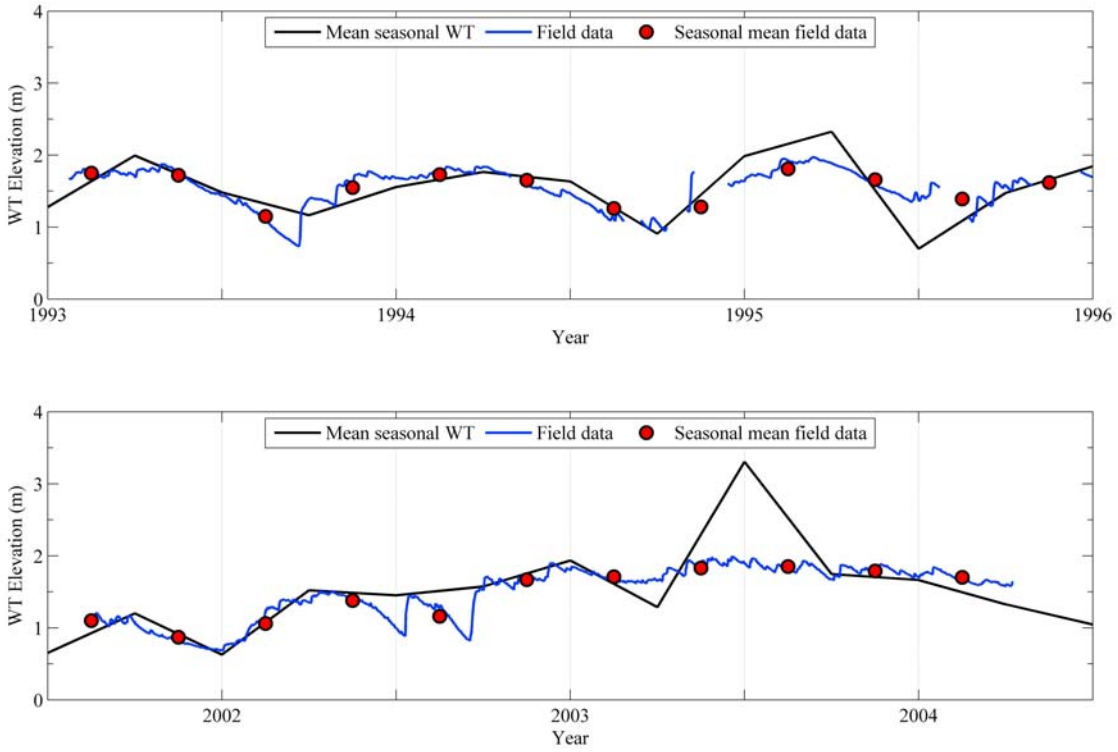

Figure 5. Comparison of simulated seasonal water table (WT) elevations and field measurements during (top) 1993–1996 and (bottom) 2001–2004.

groundwater discharge velocity to Pamlico Sound are similar at the same lags and range from 17.6% to 23.9%. SGR in both Pamlico Sound and the Atlantic Ocean shows similar winter patterns of up to 5 months lag (Spearman's ρ ranging from 0.33 to 0.27). Anomalies in SGR to the Atlantic Ocean indicate variations of 6.1% to 9.3% between 0 and 5 months lag, while anomalies in SGR to Pamlico Sound are slightly higher at the same lags and range from 7.9% to 12.7%.

[24] Spring results are much less suggestive of ENSO influence both in terms of correlations (Spearman's ρ) and anomalies. Water table elevations show significant correlations ($p < 0.05$) at no lag (Spearman's ρ of 0.29). Water table anomalies indicate a variation of 4.2% at no lag. Simulated groundwater discharge velocities in the nearshore of Pamlico Sound and the Atlantic Ocean show significant correlations of 0 to 1 month lag (Spearman's ρ ranging from 0.40 to 0.28). Anomalies in groundwater discharge velocity to the Atlantic Ocean indicate variations of 7.5% at no lag. Anomalies in groundwater discharge velocity to Pamlico Sound are similar at the same lag with an anomaly of 6.8%.

3.2. Generic Model

[25] The generic model simulations are meant to test a smaller model domain in more detail. The finer mesh enables us to break out freshwater SGD from saline circulation, thereby allowing us to look at correlations between freshwater SGD and MEI. These simulations are also meant to be used for comparison with the results of *Michael et al.* [2005], who used a similar model domain to examine seasonal oscillations in SGD using a sinusoidal recharge rate. The generic simulations show that the ENSO signal significantly influences winter and spring freshwater SGD and SGR at several lags.

[26] Figure 6 shows the simulation results for the base scenario of the generic coastal aquifer model. Because the grid spacing is finer for these sensitivity simulations than it is for the Hatteras Island simulations, the SGD signal can be broken into fresh and saline components. The fresh signal in Figure 6a is set at a total dissolved solids content that is less than 50% that of seawater; however, the correlation calculations also explore defining the fresh component of SGD at 20% and 80% of the total dissolved solids in seawater. Freshwater SGD makes up greater than 80% of total SGD when comparing the mean seasonal values as calculated from the 100 Monte Carlo simulations (Figure 6a). In a similar fashion to the Hatteras Island simulations, SGR is inversely related to SGD. Figures 6b through Figure 6d show simulation realizations and means for SGD, freshwater SGD, and SGR. The mean value of total SGD based on all 100 Monte Carlo simulations is 2.0 m^2/d (Figure 6b). This value is smaller than that simulated for Hatteras Island, owing to the lower permeability of the generic aquifer. The mean value of the freshwater component of SGD based on the 50% definition of freshwater is approximately 1.6 m^2/d (Figure 6c). Figure 6c also shows mean freshwater SGD time series under the 20% and 80% definitions of seawater. Note that the time series of freshwater SGD using the 20% definition of freshwater has a higher amplitude than those of the other two mean time series, which may explain the high correlations between the 20% definition of seawater freshwater SGD and the ENSO signal. The mean SGR rate (Figure 6d) based on the 100 Monte Carlo realizations is approximately 0.4 m^2/d, which is much smaller in com-

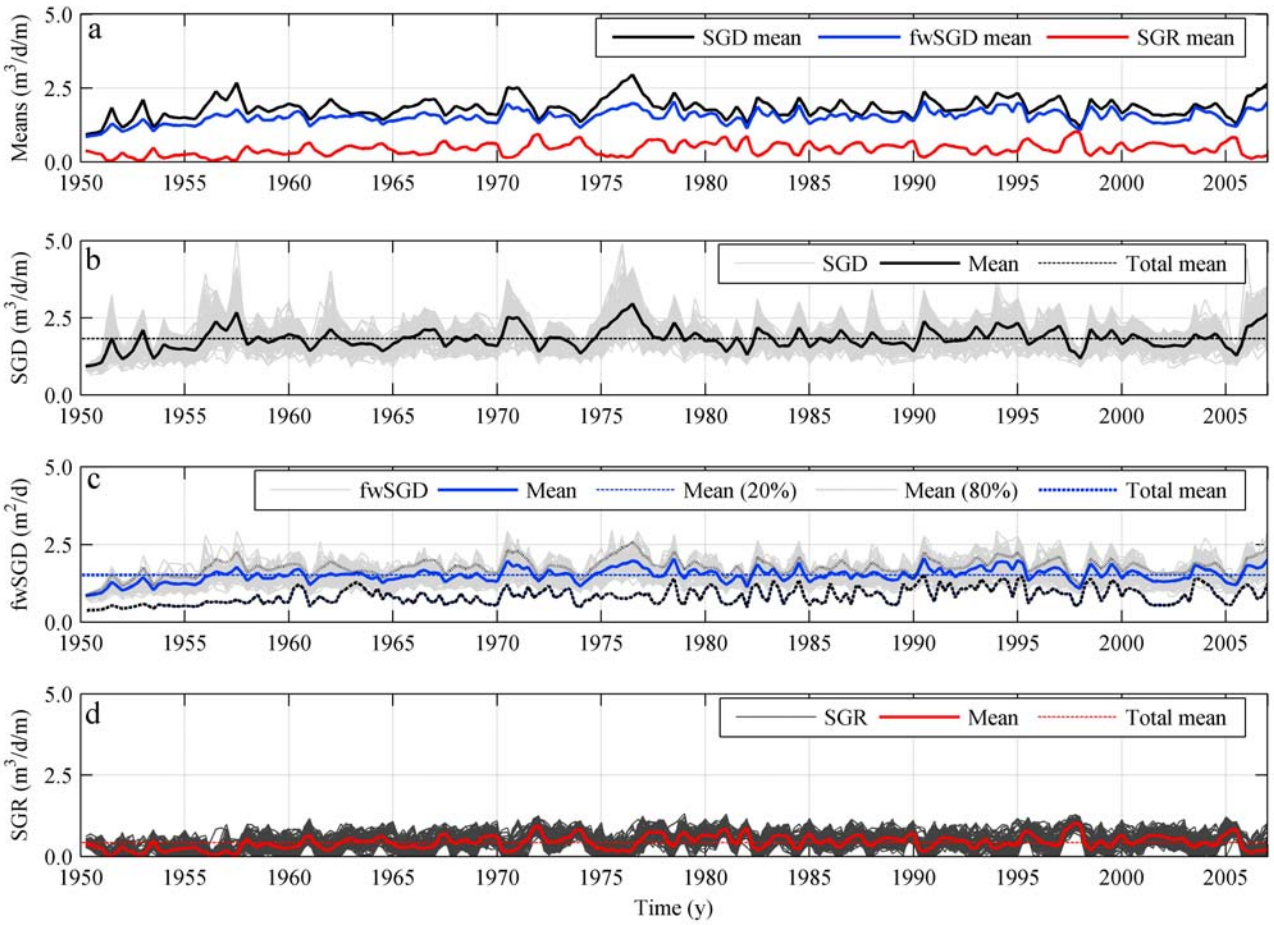

Figure 6. Generic model simulation results. (a) Simulated SGD (black line), freshwater (fw) SGD with 50% mixing (blue line), and SGR (red line) means. (b) Monte Carlo realizations (gray lines), mean (solid black line), and total mean (black dashed line) of simulated SGD. (c) Monte Carlo realizations (gray lines), mean (blue line), and total mean (blue dashed line) of simulated freshwater SGD assuming 50% mixing. Also shown are freshwater SGD assuming 20% mixing (black dashed line) and 80% mixing (gray dashed line). (d) Monte Carlo realizations (gray lines), mean (red solid line), and total mean (red dashed line) of simulated SGR.

parison with total SGD than was observed in the Hatteras Island time series, where it discharges at a rate of 70% of total SGD.

[27] The simulation results show that the 20% definition of freshwater SGD and SGR correlate significantly ($p < 0.05$) with ENSO, as expressed by MEI (Table 4). Simulated freshwater SGD (20% definition of freshwater) in the nearshore of the generic model shows significant winter correlations (all $p < 0.004$) of up to 5 months lag (Spearman's ρ ranging from 0.43 to 0.39), and no lag in spring correlations (Spearman's ρ of 0.28). Freshwater SGD anomalies (20% definition of freshwater) between the upper and lower quartiles of the MEI signal are large, with winter variations of 25.3% to 31.5% between 0 and 5 months lag and spring variations of 19.2% at no lag. SGR in the generic model's nearshore shows correlations similar to those of Hatteras Island, with significant winter correlations of up to 5 months lag (Spearman's ρ ranging from 0.30 to 0.28). SGR anomalies in the generic model are also large; winter values range from 20.1% to 35.0% between 0 and 5 months lag and the spring value is 31.4% at no lag. Because the same fundamental recharge signal has been used in both the generic model and the Hatteras Island model, we expect ENSO to exert a significant influence on several parameters in the generic model; however, it is important to note that the mean of this signal has been scaled to match that of

Table 4. Significant ENSO Correlations for $p < 0.05$ for the Generic Model Simulations

	Lag (months)					
	0	1	2	3	4	5
SGD (20%)[a]						
Winter	0.43[b]	0.42	0.41	0.40	0.38	0.39
Spring	0.28	-	-	-	-	-
SGD (50%)						
Winter	-	-	-	-	-	-
Spring	-	-	-	-	-	-
SGD (80%)						
Winter	-	-	-	-	-	-
Spring	-	-	-	-	-	-
SGR						
Winter	0.30	0.27	0.26	0.31	0.32	0.29
Spring	0.28	0.28	-	-	-	-

[a] % mixing is shown in parentheses.
[b] All significant correlations are shown as values of Spearman's ρ.

Table 5. Generic Model Parameters for Sensitivity Simulations

Parameter	Value
Base permeability (m^2)	1.0×10^{-11}
High permeability (m^2)	1.0×10^{-10}
Low permeability (m^2)	1.0×10^{-12}
Base recharge mean (kg/s)	2.3×10^{-07}
High recharge mean (kg/s)	2.9×10^{-07}
Low recharge mean (kg/s)	1.7×10^{-07}
Base model thickness (m)	20
High model thickness (m)	100

Michael et al. [2005] and that the permeability of the generic model domain is lower than that of Hatteras Island.

[28] The modeling results to this point suggest that freshwater SGD and SGR may be influenced by ENSO-derived variations in aquifer recharge, and these correlations have been demonstrated with models of different permeability and aquifer thickness. In an effort to explore further the role that aquifer parameters may exert on the potential correlation between the ENSO signal, freshwater SGD, and SGR, we varied values for permeability, recharge rate, and aquifer thickness in the manner of *Michael et al.* [2005] (Table 5). First, permeability is increased and decreased by an order of magnitude. Under both scenarios, significant correlations exist only in the SGR signal (Table 6). Using higher permeabilities, these correlations are roughly the same as the base scenario, although significant spring lags extend to 2 months and fall lags of 5 months are also significant. With lower permeabilities, nearly all significance disappears and SGR shows a significant winter correlation at only 0, 4, and 5 months lag (Spearman's ρ ranging from 0.28 to 0.26). Next, recharge is varied by altering the time series mean by 25%. Under the high-recharge scenario, all significance disappears. Under the low-recharge scenario, ENSO-correlated significance occurs only at 0, 3, 4, and 5 months lag in winter (Spearman's ρ ranging from 0.32 to 0.27), 0 and 1 month lag in spring (Spearman's ρ of 0.29), and 5 months lag in fall (Spearman's ρ of 0.27). Finally, the thickness of the aquifer is increased to 100 m. Both freshwater SGD with 50% and 80% definition of freshwater and total SGD now show some level of significant correlation with ENSO. The 50% definition of freshwater model of freshwater SGD shows significant winter correlations from 0 to 5 months lag (Spearman's ρ ranging from 0.49 to 0.31) and significant spring correlations from 0 to 3 months lag (Spearman's ρ ranging from 0.44 to 0.32). The 80% definition of freshwater model shows significant correlations in winter at 5 months lag (Spearman's ρ of 0.31) and in spring at 2 months lag (Spearman's ρ of 0.28). Total SGD, which combines fresh and saline groundwater circulation, shows significant negative winter correlation at 4 months lag (Spearman's ρ of −0.27). The SGR signal shows significance at all winter lags except 2 months (Spearman's ρ ranging from 0.33 to 0.26).

4. Discussion

[29] We begin our discussion with a question: Can the results of these numerical simulations be generalized among all coastal aquifers? In an effort to answer this question, Table 7 shows several typical barrier island aquifer parameters for a range of islands along the Atlantic and Gulf Coastal Plain physiographic provinces. These parameters derive from values documented in the literature for a range of barrier island types. The values of the parameters in Table 7 and those referenced by *Wilson et al.* [2008] are all in the range of those used in the generic model. The hydraulic conductivities used in the numerical experiments (converted from permeability to 7.5 m/d in the generic model and 20.7 m/d in the Hatteras Island model) are typical of the range found in the sampled barrier island aquifers (Table 7). Only one permeability value, from St. George Island, Florida [*Corbett et al.*, 2000], is an order of magnitude greater than the simulated values, a value at which the sensitivity analyses suggest the ENSO correlations would break down. The recharge rates simulated in this study are larger than those documented in the literature by factors ranging from 4 to 10. While the sensitivity simulations suggest that ENSO correlations break down at low mean seasonal recharge rates, this phenomenon must be combined with permeability to fully assess the impact on these low-recharge, and presumably, low-permeability aquifers. The values of Holocene thickness are all of the same order of magnitude as the generic model, suggesting that the largest aquifer thickness in the sensitivity study is outside the typical range of natural thicknesses. On the basis of these documented values, we are confident that the numerical experiments utilize aquifer parameters that are typical of many barrier island and coastal aquifers with similar parameters.

[30] Another question concerns the lags between the model output and the MEI signal: Do the lags shown in this study diminish from winter to spring because of decay in the teleconnection between ENSO and precipitation or do they diminish as the result of the aquifer's ability to filter out the signal? One explanation is that there may not be a teleconnection of the ENSO signal beyond the winter season. Another explanation concerns the effects of the aquifer on the potential ENSO-induced precipitation. This study demonstrates that the seasonal recharge fraction at the Hatteras Island field site is essentially a step function with

Table 6. Significant ENSO Correlations for $p < 0.05$ for the Generic Model Sensitivity Simulations

	Lag (months)					
	0	1	2	3	4	5
Freshwater SGD (50% mixing), high depth						
Winter	0.31[a]	0.32	0.38	0.46	0.47	0.49
Spring	0.44	0.42	0.40	0.32	-	-
Freshwater SGD (80% mixing), high depth						
Winter	-	-	-	-	-	0.31
Spring	-	-	0.28	-	-	-
Total SGD, high depth						
Winter	-	-	-	-	−0.27	-
SGR, high permeability[b]						
Winter	0.31	0.27	-	0.32	0.32	-
Spring	0.34	0.35	0.30	-	-	-
SGR, low permeability						
Winter	0.26	-	-	-	0.28	0.27
SGR, low recharge[b]						
Winter	0.29	-	-	0.31	0.32	0.27
Spring	0.29	0.29	-	-	-	-
SGR, high depth						
Winter	0.29	0.26	-	0.33	0.32	0.27

[a]All significant correlations are shown as values of Spearman's ρ.

[b]Also includes a significant fall correlation at 5 months lag with a Spearman's ρ of 0.27.

Table 7. Typical Barrier Island Aquifer Parameters

Island	Reference	Hydraulic Conductivity (m/day)	Estimated Maximum Recharge Rate (m/yr)	Approximate Holocene Thickness (m)
Generic barrier island	*Michael et al.* [2005] and current study	7.5	0.73	20.0–100.0
Hatteras Island, North Carolina	current study, *Burkett* [1996], and *Anderson and Lauer* [2008]	20.7	0.79	24.0
	Harris [1967]	12.1[a]	-	11.0
	Heath [1988]	13.8	0.50	11.0
Fire Island, New York	*Bokuniewicz and Pavlik* [1999]	60	0.56	2.0
Grand Isle, Louisiana	*Collins and Easley* [1999]	1.0–2.2	0.013–0.254	4.5–6.0
St. George Island, Florida	*Corbett et al.* [2000]	3.0–180.0	-	-
	Ruppel et al. [2000]	0.6–76.9	0.08	6.0–9.0
Sapelo Island, Georgia	*Schultz and Ruppel* [2002]	1.1–9.5[b]	-	-

[a]Estimated from pumping yields given in gal/min.
[b]Field-scale hydraulic conductivity; the paper also gives laboratory-scale values.

large and nearly equal values in winter and spring, and small and nearly equal values in summer and autumn (Table 1). The lower recharge fraction of summer and autumn reduces the amount of recharge to the aquifer during these seasons, which, in effect, reduces the strength of the ENSO signal transmitted into the aquifer by infiltration of precipitation and also reduces the strength of any remaining signal transmitted to SGD because of reduced hydraulic gradient in the aquifer. The resulting SGD, then, will not vary significantly from year to year and correlations with ENSO may not be significant. Because the recharge fraction is large in winter, any ENSO-influenced change in precipitation will affect recharge, thereby producing enough signal variation for correlations to be significant. The spring season is a different matter. Spring exhibits the largest recharge fraction of any of the seasons and is nearly twice the value that was calibrated to the summer data. However, unlike the winter months, when evapotranspiration conditions are similar during all 3 months, spring represents a transition from low-evapotranspiration conditions in March to relatively high-evapotranspiration conditions in May. Significant correlations for lagged spring model output may not be possible because of these changing conditions.

5. Conclusions

[31] The numerical experiments of this study demonstrate that ENSO-influenced climatic oscillations should affect groundwater conditions within coastal aquifers such as Hatteras Island in eastern North Carolina and in the generic conceptual model of *Michael et al.* [2005]. The simulations demonstrate further that these climatic oscillations show significant correlations with the size and shape of the subterranean estuary [*Moore*, 1999], including SGR and the freshwater component of SGD. We calculate anomalies between the upper and lower quartiles of MEI and SGR and freshwater SGD of 35.0% and 31.5%, respectively. These anomalies have important implications for nutrient loading in the nearshore of ENSO-influenced coastal aquifers, as *Michael et al.* [2005] suggest for seasonally influenced aquifers. The ENSO-derived correlations demonstrated with these numerical experiments, coupled with the potential for seasonal [*Michael et al.*, 2005] and extreme storm influences [*Anderson and Lauer*, 2008], indicate that the subterranean estuary is a highly dynamic entity in which the freshwater component of SGD varies at a range of temporal scales.

[32] The sensitivity analyses suggest that freshwater SGD and SGR exhibit significant correlations with ENSO under a fairly narrow range of aquifer permeabilities, recharge rates, and thicknesses. For example, the Hatteras Island model shows significant correlation with MEI in winter and spring under a range of lags for water table elevation, discharge velocity, and SGR. The generic model shows significant correlation with MEI in winter and spring for freshwater SGD (20% definition of freshwater) and SGR. These correlations break down, however, at higher and lower permeabilities (varied by an order of magnitude from the base scenario), higher and lower mean recharge rates (varied by 25% from the base scenario), and added aquifer thickness (increased to 100 m). This breakdown in correlation begs the following question: Is ENSO correlation an isolated phenomenon for the barrier islands of North Carolina, or is it regionally applicable?

[33] This question is important because seasonal precipitation determines the seasonal recharge rates that are used in the numerical experiments. These precipitation values, which in the generic model are a slightly modified version of the Hatteras Island precipitation record, have been demonstrated to have significant correlation with ENSO through the MEI [*Anderson and Emanuel*, 2008]. This is not an isolated phenomenon, however, because *Kurtzman and Scanlon* [2007] demonstrate that a "Wet El Niño Winter" region of high correlation between precipitation and ENSO in the form of the Southern Oscillation Index (SOI) exists throughout the Atlantic and Gulf Coastal Plains of the southeastern United States. They also show that these regions experience winter precipitation anomalies between the upper and lower quartiles of SOI of from 10% to 50%, or 75 to 227 mm. Thus, the modeling results may extend to barrier islands along these ENSO-influenced coasts and other coastal aquifers having physical characteristics (e.g., permeability, mean recharge rate, and thickness) similar to those in the numerical simulations.

[34] The results of the numerical experiments represent typical barrier island aquifer parameters, and the simulated values of total SGD, freshwater SGD, and SGR compare favorably with those in the literature [*Li et al.*, 1999; *Michael et al.*, 2005]. We deem it important to reiterate that the freshwater SGD component of the total circulation in the nearshore is the conduit for the transfer of land-sourced

contaminants to the nearshore. This component of SGD mixes with saline pore fluids of the marine SGD and SGR, which are highly enriched in nutrients [*Moore and Shaw*, 1998; *Krest et al.*, 2000]. We demonstrate in this paper that ENSO and other interannual climate signals influence the rate at which freshwater SGD flows to the subterranean estuary, thereby affecting mixing within the subterranean estuary and the biogeochemistry of the nearshore environment. ENSO-correlative regions exist along significant segments of the eastern coastline of the United States, including much of the Atlantic and Gulf Coastal Plain physiographic provinces [*Kurtzman and Scanlon*, 2007]. Given the prominence of the anomalies in freshwater SGD and SGR demonstrated with the numerical experiments, it is important that these potential variations in SGD be accounted for when assessing nutrient input to the nearshore of these aquifers.

[35] **Acknowledgments.** The authors would like to thank the three anonymous reviewers and the Associate Editor, whose insights helped to improve the manuscript. The authors would like to thank the Thomas F. and Kate M. Jeffress Memorial Trust for funding a portion of this study. We also thank Scott Marshall (Appalachian State University) for his help with model automation.

References

Anderson, W. P., Jr., and R. E. Emanuel (2008), Effect of interannual and interdecadal climate oscillations on groundwater in North Carolina, *Geophys. Res. Lett.*, *35*, L23402, doi:10.1029/2008GL036054.

Anderson, W. P., Jr., and D. G. Evans (2007), On the interpretation of recharge estimates from steady-state model calibrations, *Ground Water*, *45*(4), 499–505, doi:10.1111/j.1745-6584.2007.00312.x.

Anderson, W. P., Jr., and R. M. Lauer (2008), The role of overwash in the evolution of mixing zone morphology within barrier islands, *Hydrogeol. J.*, *16*, 1483–1495, doi:10.1007/s10040-008-0340-z.

Anderson, W. P., Jr., D. G. Evans, and S. W. Snyder (2000), The effects of Holocene barrier-island evolution on water-table elevations, Hatteras Island, North Carolina, USA, *Hydrogeol. J.*, *8*, 390–404, doi:10.1007/s100400000081.

Beebee, R. A., and M. Manga (2004), Variation in the relationship between snowmelt runoff in Oregon and ENSO and PDO, *J. Am. Water Resour. Assoc.*, *40*(4), 1011–1024, doi:10.1111/j.1752-1688.2004.tb01063.x.

Bokuniewicz, H., and B. Pavlik (1999), Groundwater seepage along a barrier island, *Biodegradation*, *10*, 257–276, doi:10.1007/BF00003147.

Burkett, C. A. (1996), Estimating the hydrogeologic characteristics of the Buxton Woods Aquifer, Hatteras Island, North Carolina, M.Sc. thesis, N. C. State Univ., Raleigh.

Burnett, W. C., et al. (2006), Quantifying submarine groundwater discharge in the coastal zone via multiple methods, *Sci. Total Environ.*, *367*, 498–543, doi:10.1016/j.scitotenv.2006.05.009.

Collins, W. H., III, and D. H. Easley (1999), Fresh-water lens formation in an unconfined barrier-island aquifer, *J. Am. Water Resour. Assoc.*, *35*(1), 1–21, doi:10.1111/j.1752-1688.1999.tb05448.x.

Corbett, D. R., K. Dillon, and W. Burnett (2000), Tracing groundwater flow on a barrier island in the north-east Gulf of Mexico, *Estuarine Coastal Shelf Sci.*, *51*, 227–242, doi:10.1006/ecss.2000.0606.

D'Odorico, P., J.-C. Yoo, and T. M. Over (2001), An assessment of ENSO-induced patterns of rainfall erosivity in the southwestern United States, *J. Clim.*, *14*, 4230–4242, doi:10.1175/1520-0442(2001)014<4230:AAOEIP>2.0.CO;2.

Drexler, J. Z., and K. C. Ewel (2001), Effect of the 1997–1998 ENSO-related drought on hydrology and salinity in a Micronesian wetland complex, *Estuaries*, *24*(3), 347–356, doi:10.2307/1353237.

Fleming, S. W., and E. J. Quilty (2006), Aquifer responses to El Niño–Southern Oscillation, southwest British Columbia, *Ground Water*, *44*(4), 595–599, doi:10.1111/j.1745-6584.2006.00187.x.

Hanson, R. T., M. W. Newhouse, and M. D. Dettinger (2004), A methodology to assess relations between climatic variability and variations in hydrologic time series in the southwestern United States, *J. Hydrol. Amsterdam*, *287*, 252–269, doi:10.1016/j.jhydrol.2003.10.006.

Harris, W. H. (1967), Stratification of fresh and salt water on barrier islands as a result of differences in sediment permeability, *Water Resour. Res.*, *3*(1), 89–97, doi:10.1029/WR003i001p00089.

Heath, R. C. (1988), Groundwater resources of the Cape Hatteras area of North Carolina: A report to the Cape Hatteras Water Association, Inc., 129 pp., Cape Hatteras Water Assoc., Buxton, N. C.

Kohout, F. (1960), Cyclic flow of salt water in the Biscayne aquifer of southeastern Florida, *J. Geophys. Res.*, *65*(7), 2133–2141, doi:10.1029/JZ065i007p02133.

Krest, J. M., W. S. Moore, L. R. Gardner, and J. T. Morris (2000), Marsh nutrient export supplied by groundwater discharge: Evidence from radium measurements, *Global Biogeochem. Cycles*, *14*(1), 167–176, doi:10.1029/1999GB001197.

Kurtzman, D., and B. R. Scanlon (2007), El Niño–Southern Oscillation and Pacific Decadal Oscillation impacts on precipitation in the southern and central United States: Evaluation of spatial distribution and predictions, *Water Resour. Res.*, *43*, W10427, doi:10.1029/2007WR005863.

Li, L., D. A. Barry, F. Stagnitti, and J.-Y. Parlange (1999), Submarine groundwater discharge and associated chemical input to a coastal sea, *Water Resour. Res.*, *35*(11), 3253–3259, doi:10.1029/1999WR900189.

Li, L., D. A. Barry, F. Stagnitti, and J.-Y. Parlange (2000), Groundwater waves in a coastal aquifer: A new governing equation including vertical effects and capillarity, *Water Resour. Res.*, *36*(2), 411–420, doi:10.1029/1999WR900307.

Michael, H. A., J. S. Lubetsky, and C. F. Harvey (2003), Characterizing submarine groundwater discharge: A seepage meter study in Waquoit Bay, Massachusetts, *Geophys. Res. Lett.*, *30*(6), 1297, doi:10.1029/2002GL016000.

Michael, H. A., A. E. Mulligan, and C. F. Harvey (2005), Seasonal oscillations in water exchange between aquifers and the coastal ocean, *Nature*, *436*, 1145–1148, doi:10.1038/nature03935.

Moore, W. S. (1996), Large groundwater inputs to coastal waters revealed by ^{226}Ra enrichments, *Nature*, *380*, 612–614, doi:10.1038/380612a0.

Moore, W. S. (1999), The subterranean estuary: A reaction zone of ground water and sea water, *Mar. Chem.*, *65*, 111–125, doi:10.1016/S0304-4203(99)00014-6.

Moore, W. S., and T. J. Shaw (1998), Chemical signals from submarine fluid advection onto the continental shelf, *J. Geophys. Res.*, *103*(C10), 21,543–21,552, doi:10.1029/98JC02232.

Moore, W. S., and A. M. Wilson (2005), Advective flow through the upper continental shelf driven by storms, buoyancy, and submarine groundwater discharge, *Earth Planet. Sci. Lett.*, *235*, 564–576, doi:10.1016/j.epsl.2005.04.043.

Moore, W. S., J. Krest, G. Taylor, E. Roggenstein, S. Joye, and R. Lee (2002), Thermal evidence of water exchange through a coastal aquifer: Implications for nutrient fluxes, *Geophys. Res. Lett.*, *29*(14), 1704, doi:10.1029/2002GL014923.

Mulligan, A. E., and M. A. Charette (2006), Intercomparison of submarine groundwater discharge estimates from a sandy unconfined aquifer, *J. Hydrol. Amsterdam*, *327*, 411–425, doi:10.1016/j.jhydrol.2005.11.056.

Prieto, C., and G. Destouni (2005), Quantifying hydrological and tidal influences on groundwater discharges into coastal waters, *Water Resour. Res.*, *41*, W12427, doi:10.1029/2004WR003920.

Rajagopalan, B., and U. Lall (1998), Interannual variability in western US precipitation, *J. Hydrol. Amsterdam*, *210*, 51–67, doi:10.1016/S0022-1694(98)00184-X.

Rodell, M., and J. S. Famiglietti (2001), An analysis of terrestrial water storage variations in Illinois with implications for the Gravity Recovery and Climate Experiment (GRACE), *Water Resour. Res.*, *37*(5), 1327–1339, doi:10.1029/2000WR900306.

Ruppel, C., G. Schultz, and S. Kruse (2000), Anomalous fresh water lens morphology on a strip barrier island, *Ground Water*, *38*(6), 872–881, doi:10.1111/j.1745-6584.2000.tb00686.x.

Schultz, G., and C. Ruppel (2002), Constraints on hydraulic parameters and implications for groundwater flux across the upland-estuary interface, *J. Hydrol. Amsterdam*, *260*, 255–269, doi:10.1016/S0022-1694(01)00616-3.

Smith, A. J. (2004), Mixed convection and density-dependent seawater circulation in coastal aquifers, *Water Resour. Res.*, *40*, W08309, doi:10.1029/2003WR002977.

Smith, C. G., J. E. Cable, and J. B. Martin (2008), Episodic high intensity mixing events in a subterranean estuary: Effects of tropical cyclones, *Limnol. Oceanogr.*, *53*(2), 666–674.

Stallman, R. W. (1965), Steady one-dimensional fluid flow in a semi-infinite porous medium with sinusoidal surface temperature, *J. Geophys. Res.*, *70*(12), 2821–2827, doi:10.1029/JZ070i012p02821.

Suzuki, S. (1960), Percolation measurements based on heat flow through soil with special reference to paddy fields, *J. Geophys. Res.*, *65*(9), 2883–2885, doi:10.1029/JZ065i009p02883.

Taniguchi, M. (2002), Tidal effects on submarine groundwater discharge into the ocean, *Geophys. Res. Lett.*, *29*(12), 1561, doi:10.1029/2002GL014987.

Taniguchi, M., W. C. Burnett, J. E. Cable, and J. V. Turner (2002), Investigation of submarine groundwater discharge, *Hydrol. Processes*, *16*, 2115–2129, doi:10.1002/hyp.1145.

van der Velde, M., M. Javaux, M. Vanclooster, and B. E. Clothier (2006), El Niño–Southern Oscillation determines the salinity of the freshwater lens under a coral atoll in the Pacific Ocean, *Geophys. Res. Lett.*, *33*, L21403, doi:10.1029/2006GL027748.

Voss, C. I. (1984), SUTRA: A finite-element simulation model for saturated-unsaturated fluid-density-dependent ground-water flow with energy transport or chemically reactive single-species solute transport, *U.S. Geol. Surv. Water Resour. Invest. Rep.*, *84–4369*.

Voss, C. I., and A. M. Provost (2002), A model for saturated-unsaturated, variable-density ground-water flow with solute or energy transport, *U.S. Geol. Surv. Water Resour. Invest. Rep.*, *02–4231*.

Wilson, A. M. (2003), The occurrence and chemical implications of geothermal convection of seawater in continental shelves, *Geophys. Res. Lett.*, *30*(21), 2127, doi:10.1029/2003GL018499.

Wilson, A. M., and L. R. Gardner (2006), Tidally driven groundwater flow and solute exchange in a marsh: Numerical simulations, *Water Resour. Res.*, *42*, W01405, doi:10.1029/2005WR004302.

Wilson, A. M., M. Huettel, and S. Klein (2008), Grain size and depositional environment as predictors of permeability in coastal marine sands, *Estuarine Coastal Shelf Sci.*, *80*, 193–199, doi:10.1016/j.ecss.2008.06.011.

Wolter, K., and M. S. Timlin (1998), Measuring the strength of ENSO: How does 1997/98 rank?, *Weather*, *53*, 315–324.

W. P. Anderson Jr. and R. E. Emanuel, Department of Geology, Appalachian State University, ASU Box 32067, Boone, NC 28607-2067, USA. (andersonwp@appstate.edu)